https://doi.org/10.1016/j.jsv.2017.11.026

Application of a movable active vibration control system on a floating raft

Zhen Wang, Cheuk Ming Mak *

Department of Building Services Engineering, The Hong Kong Polytechnic University, Hung Hom, Kowloon, Hong Kong

*Corresponding Author: Tel.: +852 2766 5856; Fax: +852 2765 7198

E-mail address: cheuk-ming.mak@polyu.edu.hk (C.M. Mak).

ABSTRACT

This paper presents a theoretical study of an inertial actuator connected to an accelerometer by a local feedback loop for active vibration control on a floating raft. On the criterion of the minimum power transmission from the vibratory machines to the flexible foundation in the floating raft, the best mounting positions for the inertial actuator on the intermediate mass of the floating raft are investigated. Simulation results indicate that the best mounting positions for the inertial actuator vary with frequency. To control time-varying excitations of vibratory machines on a floating raft effectively, an automatic control system based on real-time measurement of a cost function and automatically searching the best mounting position of the inertial actuator is proposed. To the best of our knowledge, it is the first time that an automatic control system is proposed to move an actuator automatically for controlling a time-varying excitation.

Keywords: Active control; inertial actuator; floating raft; vibration isolation; feedback control.

1. Introduction

Noise and vibration is a principal issue for warships and submarines. Any techniques and applications that decrease noise and vibration levels of warships and submarines by even a few decibels are worth pursuing. Floating rafts and floating floors are such applications which can reduce noise and vibration in ship cabins effectively [1]. They have been widely applied to ships [2, 3], submarines [4], and buildings [1, 5-8] to control noise and vibration transmission and therefore enhance human comfort and well-being [9].

Floating rafts and floating floors are passive control systems. Floating rafts are a kind of two stage vibration isolation system. Floating floors are a kind of vibration control system combined vibration isolation and structural damping. Vibration isolation and structural damping are the most widely used passive vibration control methods [10]. Passive vibration control methods can be successfully utilized to reduce vibration transmission in the middle and high audio frequency ranges [11]. Passive vibration control methods are effective and efficient at high frequencies but expensive and bulky at low frequencies [12]. Moreover, passive vibration control methods are sensitive to variations of excitation sources. In contrast to passive vibration control methods, active vibration control systems can be cheaper, for the same level of performance [13]. Active vibration control systems can also be smaller and lighter than passive ones. In addition, active vibration control systems have the advantage of being able to control vibration across wider bands of operating frequencies, which implies robustness to changes in operating frequencies [14]. Moreover, active vibration control systems can be integrated with adaptive algorithms, which ensure the active vibration control systems follow up the changes of time-varying systems. Passive vibration control systems are simple, while active vibration control systems contain a lot of components: sensors, actuators, power amplifier and a digital control system. Active vibration control systems are therefore much more complex than passive vibration control systems like periodic structures, which employ dispersion bands of structure-borne sound wave to control vibration transmission [15]. Another disadvantage of active vibration control systems is that external energy is consumed [16].

In practice, a passive floating raft cannot perform outstanding isolation performance in low frequencies and for time-varying excitations [17]. To improve vibration isolation performance in low frequencies, semi-active and active control technologies have been applied to floating rafts [2, 17, 18]. Niu et al. [2] proposed an active floating raft isolation system, in which active actuators were inserted between machines and the intermediate mass as well as the intermediate mass and the foundation. Daley et al. [19] developed a hybrid active-passive smart "spring machinery" mounting system that controls the rigid modes of the machinery it supports. To control time-varying excitations of machines on a floating raft effectively, Sun et al. [17] proposed to utilize adaptive dynamic vibration absorbers (DVAs). They compared the performance of the adaptive DVAs for three cases of which the adaptive DVAs were mounted on three distinct positions. Their simulation results have shown that differences existed among vibration reduction performances of adaptive DVAs mounted on distinct positions. Similarly, Hui et al. [9] pointed out that mounting positions of isolators had a considerable influence on the vibration isolation performance of floating floors. This phenomenon can be explained by that floor mobility can affect vibration isolation performance of isolators efficiently [20]. To improve performance of active vibration control system, the problem of determining the optimum mounting positions of actuators is of considerable interest in engineering [21]. A lot of works have been devoted into this field and can be classified according to the cost functions been utilized. Cost functions for determining the optimum mounting positions include maximization of controllability/observability index [22-25], maximization of control forces transmitted by actuators to the structure [26], minimization of the H_2 norm of the control system [27], minimization of the required control energy [28, 29] et al. Most of these works are focused on piezoelectric actuators [30].

The adaptive dynamic vibration absorbers utilized by Sun et al. [17] were mounted on the intermediate mass directly, do not need to react off a base structure as actuators utilized by Niu et al. [2] did, can be applied to more circumstances. Similarly, inertial actuators are free from the requirement of react off a base structure and thus present a much more appealing solution [31, 32].

Inertial actuators have been utilized to improve performances of vibration isolation systems in low frequencies [31-35] and turned out to be effective. But, vibration isolation systems in these literatures are one-stage isolation systems. In this paper, an inertial actuator is being proposed to utilize in a kind of two-stage vibration isolation system – floating rafts. Besides, to the best knowledge of the authors, there are no published works about the best mounting positions of inertial actuators utilized in vibration isolation systems. The best mounting positions of an inertial actuator on the intermediate mass of a floating raft is investigated firstly in this paper. Similar to DVAs and isolators, inertial actuators mounted at different positions on a flexible structure can show different performances. Therefore, for a time-varying excitation, it is possible to improve performance of an inertial actuator by utilizing a control system which can move the inertial actuator automatically. In this paper, a novel movable active vibration control system is firstly proposed to improve the vibration isolation performance of a floating raft. The theoretical study of the floating raft system is based on a generalized mobility/impedance-power flow mathematical model developed by Xiong et al. [36]. The criterion for selecting the best mounting positions is the minimum power transmission.

2. Methods

The model of the floating raft system with the natural coordinate system attached is shown in **Fig. 1**, where "*s*-*s*" denotes the boundary condition of simply supported. The floating raft system is consisted of five substructures: two identical rotatory machines (substructure 1), eight identical upper isolators (substructure 2), a rectangular flexible intermediate mass (substructure 3), four identical lower isolators (substructure 4), and a rectangular flexible foundation with all edges simply supported (substructure 5).

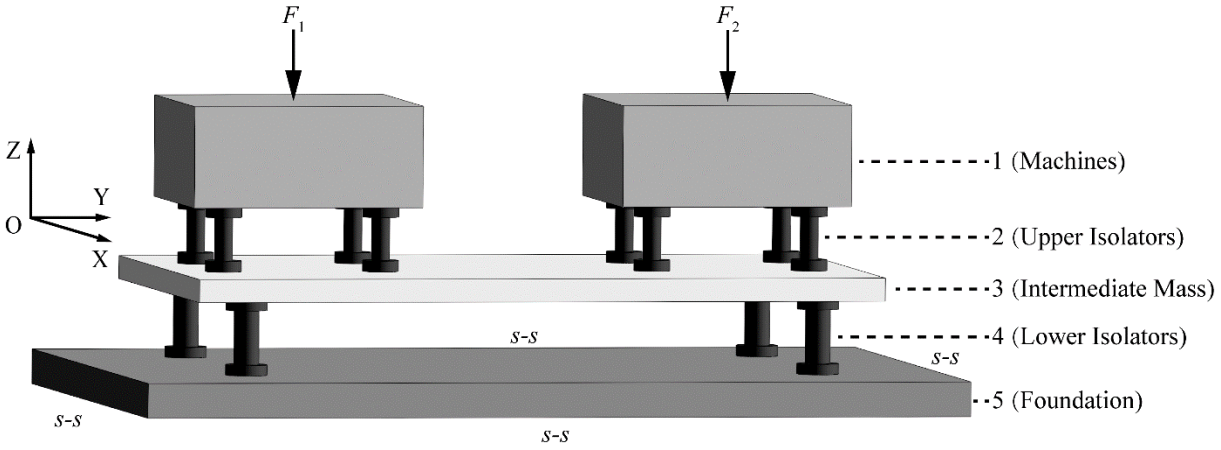

Fig. 1. A schematic diagram of the floating raft system.

In this study, it is assumed that the connections between the isolators and their connected substructures and the connection between the inertial actuator and the intermediate mass are point connections. In the calculation of the power transmission, only the force along the center axis in the Z-axis direction of the natural coordinate system as shown in **Fig. 1** is considered for simplicity.

2.1 Model of the floating raft

For the floating raft, the mobility matrix for the substructures can be expressed as

$$\begin{Bmatrix} \mathbf{V}_i^t \\ \mathbf{V}_i^b \end{Bmatrix} = \mathbf{M}_i \begin{Bmatrix} \mathbf{F}_i^t \\ \mathbf{F}_i^b \end{Bmatrix} = \begin{bmatrix} \mathbf{m}_{11}^{(i)} & \mathbf{m}_{12}^{(i)} \\ \mathbf{m}_{21}^{(i)} & \mathbf{m}_{22}^{(i)} \end{bmatrix} \begin{Bmatrix} \mathbf{F}_i^t \\ \mathbf{F}_i^b \end{Bmatrix}, \tag{1}$$

where $i = 1 \sim 5$ denote the five substructures; $\mathbf{V}_i^t$ and $\mathbf{V}_i^b$ denote the velocity vectors at the top and bottom interfaces of the ith substructure, respectively; $\mathbf{F}_i^t$ and $\mathbf{F}_i^b$ denote the force vectors at the top and bottom interfaces of the ith substructure, respectively; $\mathbf{M}_i$ denotes the governing mobility matrix between the velocity vectors and the force vectors of the ith substructure.

The two identical vibratory machines are idealized by a rectangular rigid body model of uniform mass distribution. As shown in **Fig. 2**, on the bottom interface of each machine, there are four symmetrical mounting points on the two diagonal lines. The sub-matrices of the mobility matrix $\mathbf{M}_1$ can be expressed as [37, 38]

$$\mathbf{m}_{11}^{(1)} = \frac{\mathbf{I}_2}{j\omega m_1}, \tag{2a}$$

$$\mathbf{m}_{12}^{(1)} = \frac{1}{j\omega m_1}\begin{bmatrix} 1 & 1 & 1 & 1 & 0 & 0 & 0 & 0 \\ 0 & 0 & 0 & 0 & 1 & 1 & 1 & 1 \end{bmatrix}, \tag{2b}$$

$$\mathbf{m}_{21}^{(1)} = \left[\mathbf{m}_{12}^{(1)}\right]^{\mathrm{T}}, \tag{2c}$$

$$\mathbf{m}_{22}^{(1)} = \frac{1}{j\omega m_1}\begin{bmatrix} \mathbf{s} & 0_{4\times4} \\ 0_{4\times4} & \mathbf{s} \end{bmatrix}, \tag{2d}$$

$$\mathbf{s} = \begin{bmatrix} 1+\frac{m_1 d_1^2}{8J_1} & 1-\frac{m_1 d_1^2}{8J_1} & 1 & 1 \\ 1-\frac{m_1 d_1^2}{8J_1} & 1+\frac{m_1 d_1^2}{8J_1} & 1 & 1 \\ 1 & 1 & 1+\frac{m_1 d_1^2}{8J_1} & 1-\frac{m_1 d_1^2}{8J_1} \\ 1 & 1 & 1-\frac{m_1 d_1^2}{8J_1} & 1+\frac{m_1 d_1^2}{8J_1} \end{bmatrix}, \tag{2e}$$

where j denotes the imaginary unit; ω denotes the angular frequency; m_1 denotes the mass of the vibratory machine model; $\mathbf{I}_2$ denotes a 2×2 identical matrix; the subscript T denotes the transpose of a matrix; d_1 denotes the distance between two adjacent mounting points, as shown in **Fig. 2**; J_1 denotes the moment of inertial of the vibratory machine model about its center of gravity.

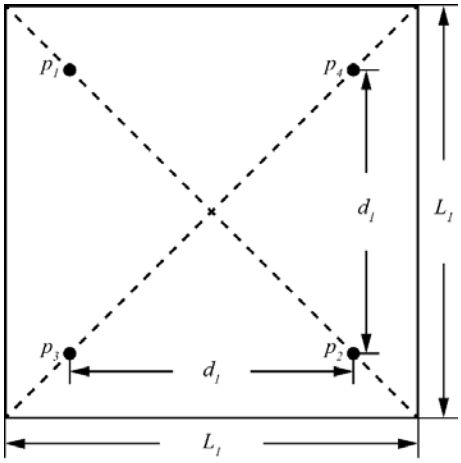

Fig. 2. A schematic diagram of the bottom interface of a machine.

The identical isolators in substructure 2 are idealized as a spring-mass-spring system with stiffness K_2 and lumped mass m_2 located at the middle of each spring as shown in **Fig. 3**. The sub-matrices of the mobility matrices $\mathbf{M}_2$ can be expressed as

$$\mathbf{m}_{11}^{(2)} = \mathbf{m}_{22}^{(2)} = \left(jw / K_2 + 1/ jwm_2 \right) \mathbf{I}_8, \tag{3a}$$

$$\mathbf{m}_{12}^{(2)} = \mathbf{m}_{21}^{(2)} = \left(1/ jwm_2 \right) \mathbf{I}_8, \tag{3b}$$

where $\mathbf{I}_8$ and $\mathbf{I}_4$ denote a 8×8 identical matrix and a 4×4 identical matrix, respectively.

Similarly, the sub-matrices of the mobility matrices $\mathbf{M}_4$ for substructure 4 can be expressed as

$$\mathbf{m}_{11}^{(4)} = \mathbf{m}_{22}^{(4)} = \left(jw / K_4 + 1/ jwm_4 \right) \mathbf{I}_4, \tag{4a}$$

$$\mathbf{m}_{12}^{(4)} = \mathbf{m}_{21}^{(4)} = \left(1/ jwm_4 \right) \mathbf{I}_4, \tag{4b}$$

where K_4 and m_4 denote the stiffness and lumped mass of a lower isolator, respectively.

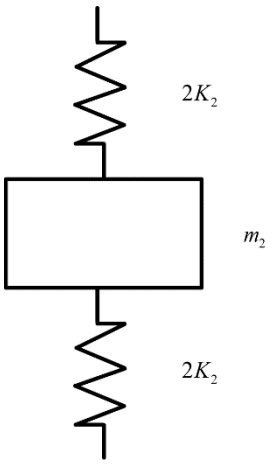

Fig. 3. A schematic diagram of the idealized isolator model.

The mobility matrices of the mounting points on the flexible intermediate mass can be solved by the modal summation method. The sub-matrices of the mobility matrix $\mathbf{M}_3$ can be expressed as

$$\mathbf{m}_{11}^{(3)} = \left[\chi_{pq}(x_p^t, y_p^t \mid x_q^t, y_q^t) \right]_{8\times 8}, \tag{5a}$$

$$\mathbf{m}_{12}^{(3)} = \left[\chi_{pq}(x_p^t, y_p^t \mid x_q^b, y_q^b) \right]_{8\times 4}, \tag{5b}$$

$$\mathbf{m}_{21}^{(3)} = \left[\chi_{pq}(x_p^b, y_p^b \mid x_q^t, y_q^t) \right]_{4\times 8}, \tag{5c}$$

$$\mathbf{m}_{22}^{(3)} = \left[\chi_{pq}(x_p^b, y_p^b \mid x_q^b, y_q^b) \right]_{4\times 4}, \tag{5d}$$

$$\chi_{pq}(x_p, y_p | x_q, y_q) = j\omega \sum_{r=1}^{\infty} \frac{\phi_r(x_p, y_p)\phi_r(x_q, y_q)}{m_3 \left[\omega_r^2 (1 + j\eta_3) - \omega^2 \right]}, \tag{5e}$$

where (x_p^t, y_p^t) and (x_q^t, y_q^t) denote the mounting positions of upper isolators on the intermediate mass; (x_p^b, y_p^b) and (x_q^b, y_q^b) denote the mounting positions of lower isolators on the intermediate mass; m_3 denotes the weight of the intermediate mass; ω_r denotes the *r*th natural frequency of the intermediate mass; $\phi_r(x_p, y_p)$ and $\phi_r(x_q, y_q)$ denote the *r*th natural mode of the intermediate mass at position with coordinates (x_p, y_p) and (x_q, y_q), respectively; η_3 denotes the loss factor of the intermediate mass.

For the flexible foundation, the mobility matrix $\mathbf{M}_5$ can be expressed as

$$\mathbf{M}_5 = [\chi_{pq}(x_p, y_p | x_q, y_q)]_{4\times 4}, \tag{6a}$$

$$\chi_{pq}(x_p, y_p | x_q, y_q) = j\omega \sum_{n=1}^{\infty} \frac{\phi_n(x_p, y_p)\phi_n(x_q, y_q)}{m_5\left[\omega_n^2(1+j\eta_5) - \omega^2\right]}, \tag{6b}$$

where (x_p, y_p) and (x_q, y_q) denote the mounting positions of the lower isolators on the flexible foundation; m_5 denotes the mass of the foundation; ω_n denote the *n*th natural frequency of the flexible foundation; $\phi_n(x_p, y_p)$ and $\phi_n(x_q, y_q)$ denote the *n*th natural mode of the flexible foundation at position with coordinates (x_p, y_p) and (x_q, y_q), respectively; η_5 denotes the loss factor of the flexible foundation.

The relationships between the transmitted forces and the corresponding velocities on the interfaces of the five substructures can be expressed as

$$\mathbf{F}_i^b = -\mathbf{F}_{i+1}^t, \tag{7}$$

$$\mathbf{V}_i^b = \mathbf{V}_{i+1}^t, \tag{8}$$

where i = 1 ~ 4. By combining Eqs. (1) to (8), the force and velocity vectors on the top interface of the foundation can be expressed as

$$\mathbf{F}_5^t = \mathbf{T}_4\mathbf{T}_3\mathbf{T}_2\mathbf{T}_1\mathbf{F}_1^t, \tag{9}$$

$$\mathbf{V}_5^t = \mathbf{M}_5\mathbf{F}_5^t, \tag{10}$$

where

$$\mathbf{T}_4 = -(\mathbf{M}_5 + \mathbf{m}_{22}^{(4)})^{-1}\mathbf{m}_{21}^{(4)}, \tag{11}$$

$$\mathbf{T}_i = -(\mathbf{m}_{11}^{(i+1)} + \mathbf{m}_{12}^{(i+1)}\mathbf{T}_{i+1} + \mathbf{m}_{22}^{(i)})^{-1}\mathbf{m}_{21}^{(i)}, \tag{12}$$

where i = 1 ~ 3. The structure-borne sound power transmission from the two vibratory machines to the flexible foundation can be expressed as [39]

$$P_f = \frac{1}{2}\mathrm{Re}((\mathbf{F}_5^t)^*\mathbf{V}_5^t)\,. \tag{13}$$

2.2 Model of the inertial actuator

An inertial actuator is a mass supported on springs and driven by an external force [33]. The external force in an inertial actuator can be generated electromagnetically [32, 33] or electromechanically [40-42]. The inertial actuator proposed in the active vibration control system is of the same type as the one utilized by Wang et al. [43], that consists of a voice coil motor and four steel springs. **Fig. 4** (a) shows the schematic diagram of the electromechanical model of the inertial actuator. In **Fig. 4** (a), m_a denotes the mass of upper part of the inertial actuator; K_a denotes the stiffness coefficient of the inertial actuator; C_a denotes the damping coefficient of the inertial actuator; ψ denotes the force factor of the voice coil motor in the inertial actuator; i_a denotes the driving current of the voice coil motor in the inertial actuator; $f_a = \psi i_a$ denotes the output force of the voice coil motor. The transmitted force and the corresponding velocity response at the connect point on the bottom interface of the inertial actuator are f_c and v_c, respectively. **Fig. 4** (b) shows the block diagram of the local feedback loop, where $G_{cc}(\omega)$ denotes the frequency response of the inertial actuator; *g* denotes the feedback gain of the feedback loop; $i_a(\omega)$ denotes the spectrum of the driven current; $\dot{v}_c(\omega)$ denotes the spectrum of the acceleration at the mounting position of the inertial actuator with control. The primary disturbance denotes the response of the intermediate mass resulted from the two identical vibratory machines in the floating raft. The secondary signal denotes the output current signal of the local feedback loop.

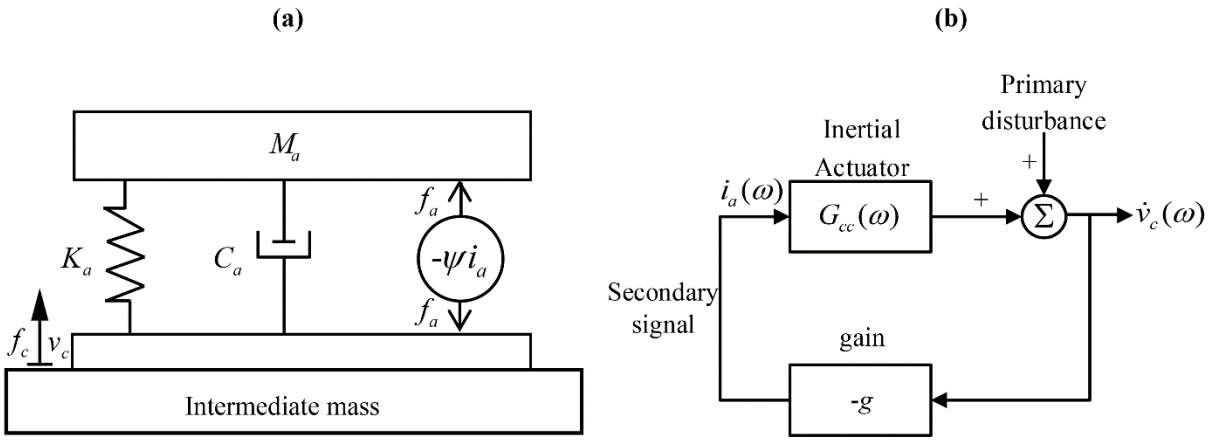

Fig. 4. Plot (a) A schematic diagram of the electromechanical model of the inertial actuator. Plot (b) A block diagram of the local feedback loop.

According to the electromechanical model described by Díaz et al. [44], the force transmitted from the inertial actuator to the intermediate mass at the connection point f_c and the frequency response of the inertial actuator $G_{cc}(\omega)$ can be expressed as

$$f_c = \frac{\psi}{1+Z_a(Y_a+Y_{cc})} i_a , \tag{14}$$

$$G_{cc}(\omega) = \frac{Y_{cc}\psi}{j\omega(1+Z_a(Y_a+Y_{cc}))} , \tag{15}$$

where $Z_a = C_a + K_a / j\omega$ denotes the mobility of the steel springs in the inertial actuator; $Y_a = 1/ j\omega m_a$ denotes the mobility of the mass m_a; Y_{cc} denotes the point mobility at the mounting position between the inertial actuator and the intermediate mass.

With the inertial actuator mounted on the intermediate mass, the governing equation between the velocity and force vectors of the intermediate mass can be rewritten as

$$\begin{Bmatrix} \mathbf{V}_3^t \\ \mathbf{V}_3^b \\ v_c \end{Bmatrix} = \begin{bmatrix} \mathbf{M}_3 & \mathbf{IA} \\ \mathbf{IA}^{\mathrm{T}} & Y_{cc} \end{bmatrix} \begin{Bmatrix} \mathbf{F}_3^t \\ \mathbf{F}_3^b \\ f_c \end{Bmatrix}, \tag{16a}$$

$$\mathbf{IA} = \left[\chi_{pq}(x_p^l, y_p^l \mid x^A, y^A) \right]_{12\times 1}, \tag{16b}$$

$$Y_{cc} = \chi_{pq}(x^A, y^A \mid x^A, y^A), \tag{16c}$$

where χ_{pq} has the same form as in Eq. (5e); (x_p^l, y_p^l) and (x^A, y^A) denote the coordinates of mounting positions for an isolator (i. e. the upper isolators or the lower isolators) and the inertial actuator on the intermediate mass.

With the acceleration feedback control implemented, the driven current in the voice coil motor is $i_a(\omega)=g\times\dot{v}_c(\omega)=g\times j\omega v_c(\omega)$. The output force of the voice coil motor can then be rewritten as

$$f_a(\omega) = -\psi i_a(\omega) = -j\omega g\psi v_c(\omega). \tag{17}$$

The spectrum of force f_c can be updated as

$$f_c(\omega) = \frac{\psi}{1+Z_a(Y_a+Y_{cc})} i_a(\omega) = \frac{j\omega g\psi}{1+Z_a(Y_a+Y_{cc})} v_c(\omega). \tag{18}$$

The spectrum of transfer mobility M_A between the velocity v_c and the force f_c at the mounting position for the inertial actuator on the top interface of the intermediate mass can be expressed as

$$M_A = \frac{v_c(\omega)}{f_c(\omega)} = \frac{1+Z_a(Y_a+Y_{cc})}{j\omega g\psi}. \tag{19}$$

By combining Eqs. (16) and (19), the force f_c and the velocity v_c in Eq. (16) can be eliminated. The governing equation for the intermediate mass can be rewritten as

$$\begin{Bmatrix} \mathbf{V}_3^t \\ \mathbf{V}_3^b \end{Bmatrix} = \mathbf{M}_3^{'} \begin{Bmatrix} \mathbf{F}_3^t \\ \mathbf{F}_3^b \end{Bmatrix}, \tag{19}$$

$$\mathbf{M}_3^{'} = \mathbf{M}_3 + \mathbf{IA}\left(M_A - Y_{cc}\right)^{-1} \mathbf{IA}^{\mathrm{T}}. \tag{20}$$

The structure-borne sound power transmitted to the flexible foundation with the inertial actuator installed on the top interface of the intermediate mass and operated can be expressed as

$$P_f^{'} = \frac{1}{2}\mathrm{Re}((\mathbf{F}_5^{t'})^* \mathbf{V}_5^{t'}), \tag{21}$$

where $\mathbf{F}_5^{t'}$ and $\mathbf{V}_5^{t'}$ denote the force and velocity vectors of the flexible foundation with the inertial actuator installed on the top interface of the intermediate mass and operated, respectively.

3. Analysis

The physical and geometrical parameters of the machines are m_1 = 30 kg, J_1 = 0.26 kg m^2, and d_1 = 0.2 m. The physical parameters of the upper isolators are m_2 = 0.25 kg, K_2 = 6.66×10^4 N/m. The physical parameters of the intermediate mass are m_3 = 75.6 kg, ρ_3 = 2.8×10^3 kg/m^3, E_3 = 2.1×10^{10} N/m^2, and η_3 = 0.02. The physical parameters of the lower isolators are m_4 = 0.4 kg, K_4 = 3.01×10^5 N/m. The physical parameters of the flexible foundation are m_5 = 567 kg, ρ_5 = 2.8×10^3 kg/m^3, E_5 = 2.1×10^{10} N/m^2, and η_5 = 0.02. The first order natural frequencies of the intermediate mass and the foundation are 82.5 Hz and 329 Hz, respectively. The physical parameters of the inertial actuator are m_a = 5 kg, K_a = 4.44×10^4 N/m, C_a = 47.1 N/ms^{-1}, and ψ = 19.8 N/A. The resonant frequency of the inertial actuator is 15 Hz.

The top view of the rectangular intermediate mass with a local rectangular coordinate system (*oxy*) attached is shown in **Fig. 5**. The eight circles filled with grey denote the mounting positions for the eight upper isolators. It is assumed that the inertial actuator can be mounted on any points along the axis of symmetric (the bold grey line shown in **Fig. 5**) on the top interface of the intermediate mass paralleled with the *x*-axis in the local rectangular coordinate system. The inertial actuator can be moved along the axis of symmetric by the automatic control system.

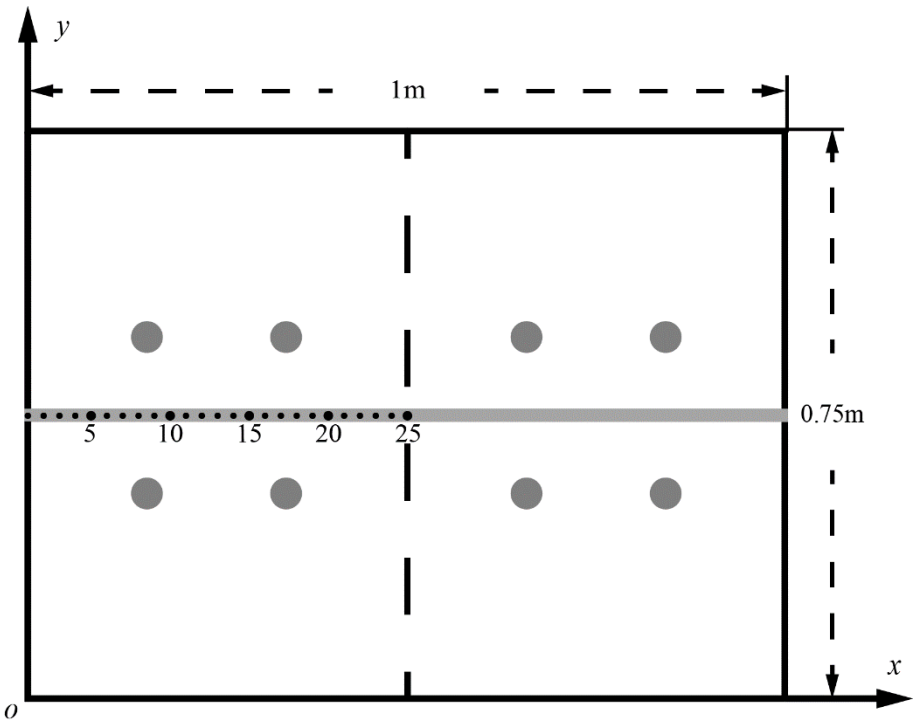

Fig. 5. A top view of the rectangular intermediate mass.

The rectangular intermediate mass is mirror symmetrical about the two axes of symmetry which parallel to the *x*-axis and the *y*-axis in the local rectangular coordinate system as shown in **Fig. 5**. Therefore, only half of the mounting positions on the axis of symmetric should be investigated. Twenty-five mounting positions (circles filled with black shown in **Fig. 5**) equally spaced along the left half of the bold grey line are studied. The numbers below the possible mounting positions denote serial numbers of the mounting positions for the inertial actuator.

For the 25 possible mounting positions, the power transmission from the two vibratory machines to the flexible foundation with and without the inertial actuator mounted on the intermediate mass are studied. In the calculation of the power transmission from the two vibratory machines to the flexible foundation, the magnitudes of the excitation force of the two identical vibratory machines are $\mathbf{F}_1^t = [1;1]$ in the frequency range from 20 Hz to 250 Hz. The natural frequencies and mode shapes of the intermediate mass are simulated by utilizing the finite element method in the enterprise software COMSOL. The natural frequencies and mode shapes of the flexible foundation with all edges simply

supported are solved by theoretical analysis method. Finite element simulation results of natural frequencies and mode shapes of the intermediate mass are utilized to calculate mobility of mounting points on the intermediate mass. Theoretical analysis results of natural frequencies and mode shapes of the flexible foundation are utilized to calculate mobility of mounting points on the flexible foundation.

On the criterion of the minimum power transmission from the two vibratory machines to the flexible foundation, the best mounting positions of the inertial actuator for each frequency in the frequency range from 20 Hz to 250 Hz with the frequency resolution of 1 Hz are searched. The results of the best mounting positions are shown in **Fig. 6**.

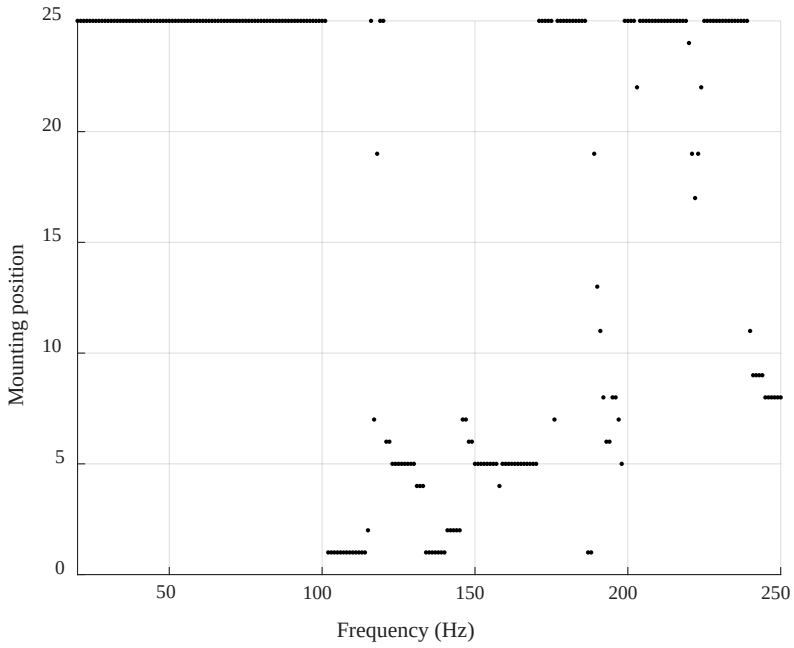

Fig. 6. Best mounting positions for the inertial actuator in the frequency range from 20 Hz to 250 Hz with the frequency resolution of 1 Hz.

Refer to **Fig. 6**, it can be found that the best mounting positions for the inertial actuator vary with frequencies. The possibility of each mounting position to be the best mounting position for the inertial actuator in the frequency range from 20 Hz to 250 Hz is calculated and shown in **Fig. 7**. The mounting position with serial number of 25 is the mounting position with the largest possibility to be the best

mounting position for the inertial actuator in the frequency range from 20 Hz to 250 Hz. It is the mounting position in the center of the top interface of the intermediate mass. Three mounting positions with possibility larger than 10% are picked out: mounting position 1, mounting position 5, and mounting position 25. The possibility of mounting position 1, mounting position 5, and mounting position 25 are 10.0%, 12.6%, and 56.0%, respectively.

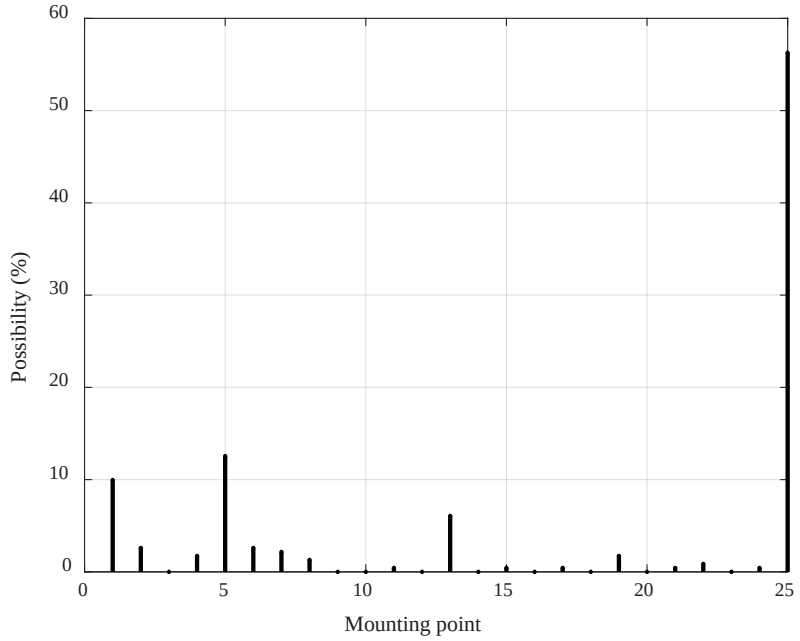

Fig. 7. Possibility of each mounting position to be the best mounting position for the inertial actuator in the frequency range from 20 Hz to 250 Hz with the frequency resolution of 1 Hz.

The magnitude of structure-borne sound power transmission from the two vibratory machines to the flexible foundation for the case without the inertial actuator mounted (thick line), the case with the inertial actuator mounted on point 1 (dashed line), the case with the inertial actuator mounted on point 5 (dotted line), and the case with the inertial actuator mounted on point 25 (thin line) are shown in **Fig. 8**. It is straightforward to find that significant differences existed among the four curves shown in **Fig. 8**. It reveals that mounting positions have a noteworthy influence on the vibration control performance of the inertial actuator. It can be found that for an inertial actuator mounted on a given position, the inertial actuator can obtain the optimum vibration control performance only in a limited frequency

range. Similarly, for an inertial actuator mounted on a position permanently, the inertial actuator can obtain the optimum vibration control performance for certain excitations. If the characteristics of the excitations vary significantly, the best mounting position for the inertial actuator should be determined again. Therefore, the strategy of moving the inertial actuator to the best mounting position corresponding to the excitations automatically have the potential of improving the broadband control performance and controlling time-varying excitations.

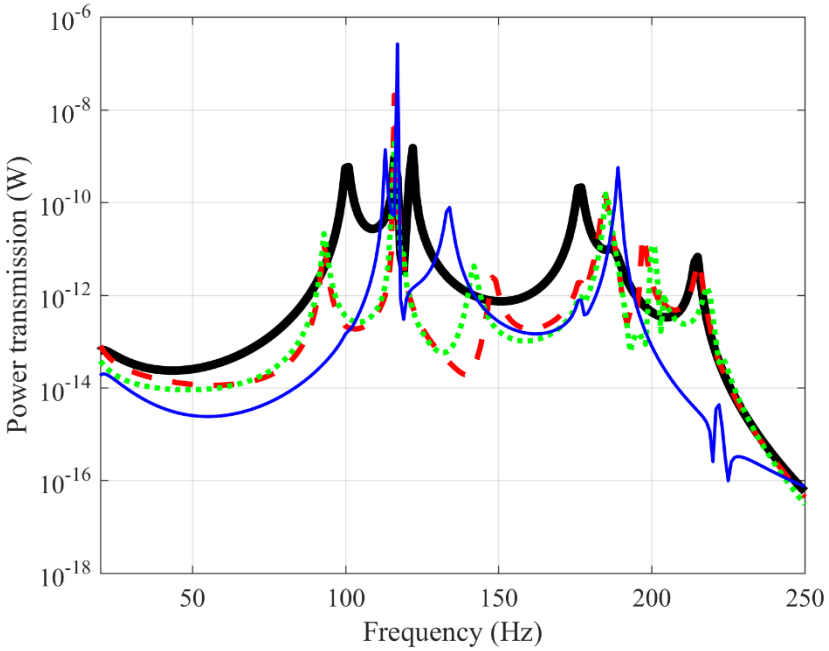

Fig. 8. (Colour online) Magnitude of structure-borne sound power transmission from the two vibratory machines to the flexible foundation: without the inertial actuator mounted on the intermediate mass (thick line), with the inertial actuator mounted on point 1 (dashed line), with the inertial actuator mounted on point 5 (dotted line), and with the inertial actuator mounted on point 25 (thin line).

4. The active control system

A movable active vibration control system consisted of a linear motor with a shaft, two tachometers, four velocity sensors (VS1 to VS4), a digital signal processing (DSP) system and an inertial actuator connected to an accelerometer by a local feedback loop is proposed. The linear motor controlled by a real-time control algorithm executed in the DSP system moves the inertial actuator automatically as

rotational speeds of the machines change with time. The schematic diagram of the floating raft system and the movable active vibration control system is shown in **Fig. 9**. The block diagram of the real-time control system is shown in **Fig. 10**.

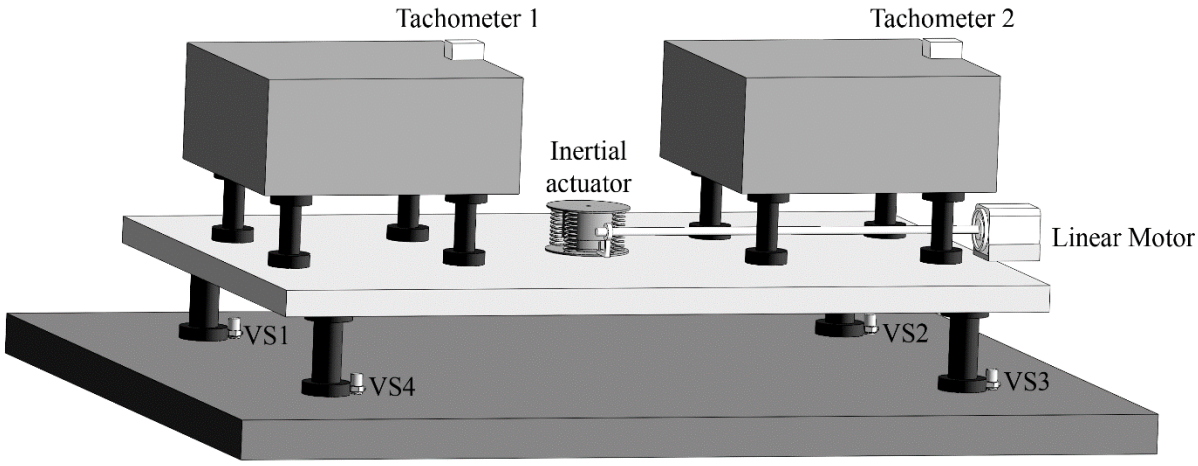

Fig. 9. A schematic diagram of the floating raft and the movable active vibration control system.

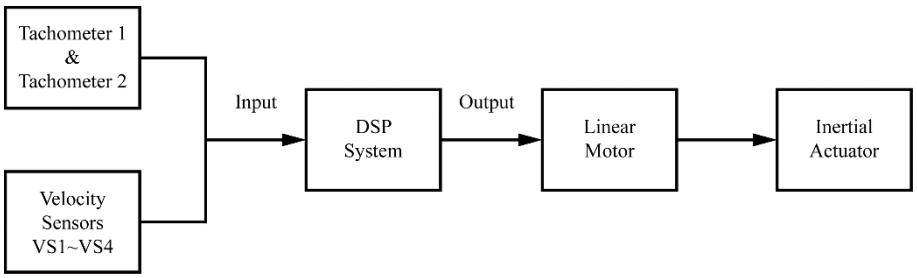

Fig. 10. A block diagram of the control system.

A control algorithm based on real-time measurement of a cost function and then automatically searched the best mounting position of the inertial actuator is proposed. The block diagram of the control algorithm of the movable active vibration control system is shown in **Fig. 11**. In **Fig. 11**, *i* and *k* are integers for counting; N_1 and N_2 denote output of tachometer 1 and tachometer 2, respectively; n = 25 denotes the amount of possible mounting positions for the inertial actuator; *mp* denotes the serial number of a possible mounting position for the inertial actuator; mod denotes the operation of

modulo; min denotes the operation of finding the minimum element in a vector or a matrix; **PS** denotes a two-dimensional matrix contains all possible values of cost function P_s; the two indices for the two-dimensional matrix **PS** are the rotational speeds of the two vibratory machines.

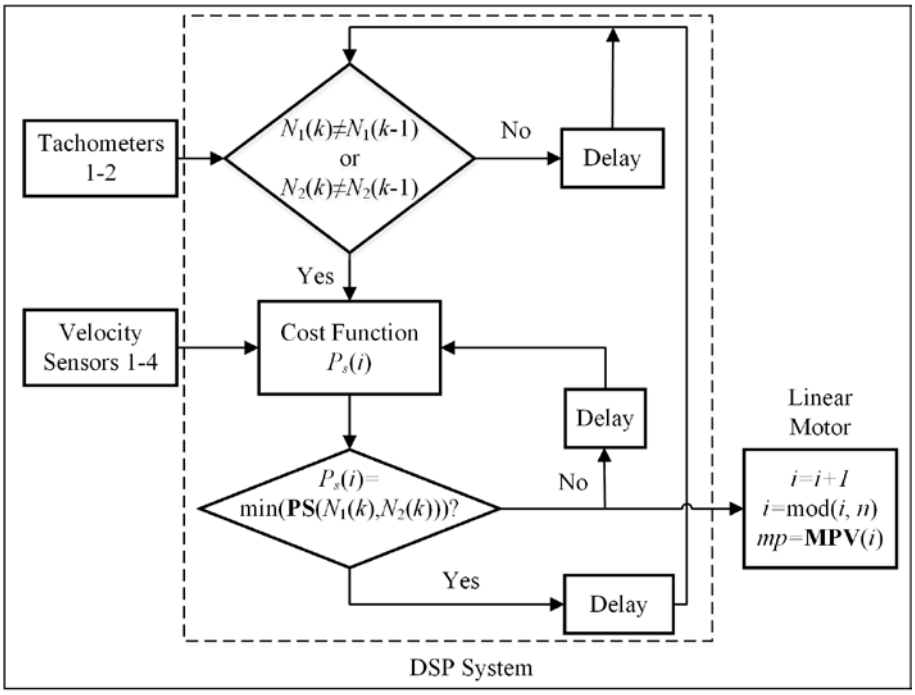

Fig. 11. A block diagram of the real-time control algorithm of the movable active vibration control system.

The DSP system monitors the rotational speeds of the two vibratory machines by real-time measurement of the output of tachometer 1 (N_1) and output of tachometer 2 (N_2). If the rotational speeds of the machines vary, the cost function P_s is then calculated with the real-time measurement result of output of the velocity sensors (VS1~VS4). The inertial actuator is moved along the axis of symmetric on the top interface of the intermediate mass from one mounting position to another mounting position by the linear motor (with a time delay larger than the time needed for calculating the cost function) until the optimization criteria is satisfied.

Cost functions or performance indexes used in active control systems include total power flows [2, 17], total kinetic energy of the controlled structure, absorbed power by the controller [45-48], et al.

The transmission of total power flows into the flexible foundation makes a straightforward illustration of the isolation performance of the floating raft system. Total power flows turned out to be an effective cost function for controllers on a floating raft [2, 17]. Excitations of machines usually contains multiple frequency components. Therefore, the time-averaged transmitted power to the flexible foundation is used as the cost function for the controller to be minimized in this control system. The velocity vector $\mathbf{V}_{\mathrm{s}} = \left[v_{s1}, v_{s2}, v_{s3}, v_{s4}\right]^{\mathrm{T}}$ measured by the four velocity sensors as shown in **Fig. 9** is used to approximate velocities ($\mathbf{V}_5^t$) at the connection points between the lower isolators and the flexible foundation. The cost function can be expressed as

$$P_{\mathrm{s}} = \frac{1}{T_0}\int_0^{T_0} \mathrm{Re}((\mathbf{V}_s/\mathbf{M}_5)^{\mathrm{T}*}\mathbf{V}_s)dt\,, \tag{23}$$

where T_0 is a time interval which is long enough to make P_{s} approaching a constant value.

5. Conclusion

This paper presents a theoretical study of the vibration control performance of a novel movable active vibration control system on a floating raft. The movable active vibration control system consists of a linear motor with a shaft, a DSP system, two tachometers, four velocity sensors, and an inertial actuator connected to an accelerometer by a local feedback loop is proposed in this paper. An algorithm based on real-time measurement of a cost function and searched the best mounting position of the inertial actuator is proposed. The criterion of the best mounting position is the minimum power transmission from the vibratory machines to the flexible foundation in the floating raft. It is validated that significant differences exist among the performances of the inertial actuator mounted at different mounting positions. The results also indicate that the best mounting positions for the inertial actuator varies with frequency. For an inertial actuator mounted at a position permanently, the inertial actuator obtains the best vibration control performance in a very limited frequency range. The results indicate that a linear motor with a shaft can be used to move the inertial actuator automatically for the

controlling of a time-varying excitation in order to achieve broadband performance.

Acknowledgements

The authors would like to thank the financial support of the Hong Kong Polytechnic University.

References

[1] I.S. Cha, H.H. Chun, Insertion loss prediction of floating floors used in ship cabins, Applied Acoustics 69 (10) (2008) 913-917.

[2] J. Niu, K. Song, C.W. Lim, On active vibration isolation of floating raft system, Journal of Sound and Vibration 285 (1–2) (2005) 391-406.

[3] A.C. Nilsson, Some acoustical properties of floating‐floor constructions, The Journal of the Acoustical Society of America 61 (6) (1977) 1533-1539.

[4] J. Pan, J.Q. Pan, C.H. Hansen, Total power flow from a vibrating rigid body to a thin panel through multiple elastic mounts, The Journal of the Acoustical Society of America 92 (2) (1992) 895-907.

[5] P.A. Nelson, Vibration isolation on floating floors, Applied Acoustics 15 (2) (1982) 97-109.

[6] A. Schiavi, A.P. Belli, M. Corallo, F. Russo. Acoustical performance characterization of resilient materials used under floating floors in dwellings, Acta Acustica united with Acustica 93 (3) (2007) 477-485.

[7] C.M. Mak, Z. Wang, Recent advances in building acoustics: An overview of prediction methods and their applications, Building and Environment 91 (2015) 118-126.

[8] H.S. Park, B.K. Oh, Y. Kim, T.J. Cho, Low-frequency impact sound transmission of floating floor: Case study of mortar bed on concrete slab with continuous interlayer, Building and Environment 94 (2015) 793-801.

[9] C.K. Hui, C.F. Ng, New floating floor design with optimum isolator location, Journal of Sound and Vibration 303 (1–2) (2007) 221-238.

[10] J. C. Malcolm, Handbook of acoustics. New York: John Wiley & Sons: 1998.

[11] F. J. Fahy, P. Gardonio, Sound and structural vibration: radiation, transmission and response. New York: Academic: 2007.

[12] M. A. Hossain, M. O. Tokhi, Evolutionary adaptive active vibration control, Proceedings of the Institute of Mechanical Engineers, Part I: Journal of Systems and Control Engineering, 211 (1997) 183-193.

[13] A. Preumont, Vibration control of active structures, an introduction, 3rd edition, New York: Springer: 2011.

[14] K. Williams, G. Chiu, and R. Bernhard, Adaptive-passive absorbers using shape-memory alloys, Journal of Sound and Vibration 249 (5) 2002 835-848.

[15] Y. Yun, C. M. Mak, A study of coupled flexural-longitudinal wave motion in a periodic dual-beam structure with transverse connection, The Journal of the Acoustical Society of America 126 (1) (2009) 114-121.

[16] K. Nakano, Y. Suda, S. Nakadai, Self-powered active vibration control using a single electric actuator, Journal of Sound and Vibration 260 (2003) 213-235.

[17] H.L. Sun, K. Zhang, P.Q. Zhang, H.B. Chen, Application of dynamic vibration absorbers in floating raft system, Applied Acoustics 71 (3) (2010) 250-257.

[18] Y.L. Li, D.L. Xu, Y.M. Fu, J.X. Zhou, Stability and chaotification of vibration isolation floating raft systems with time-delayed feedback control, Chaos: An Interdisciplinary Journal of Nonlinear Science 21 (3) (2011) 033115.

[19] S. Daley, F. A. Johnson, J. B. Pearson, R. Dixon, Active vibration control for marine applications, Control Engineering Practice, 12 (2004) 465-474.

[20] C. M. Mak, J. X. Su, A study of the effect of floor mobility on isolation efficiency of vibration isolators, Journal of low frequency noise, vibration and control effect, 20 (1) (2001) 1-13.

[21] K. R. Kumar, S. Narayanan, Active vibration control of beams with optimal placement of

piezoelectric sensor/actuator pairs, Smart Material and Structures 17 (2008) 055008.

[22] J. H. Han, I. Lee, Optimal placement of piezoelectric sensors and actuators for vibration control of a composite plate using genetic algorithms, Smart Material and Structures 8 (1999) 257-267.

[23] A. M. Sadri, J. R. Wright, R. J. Wynne, Modelling and optimal placement of piezoelectric actuators in isotropic plates using genetic algorithms, Smart Material and Structures 8 (1999) 490-498.

[24] Z. C. Qiu, X. M. Zhang, H. X. Wu, H. H. Zhang, Optimal placement and active vibration control for piezoelectric smart flexible cantilever plate, Journal of Sound and Vibration 301 (2007) 521-543.

[25] I. Bruant, L. Gallimard, S. Nikoukar, Optimal piezoelectric actuator and sensor location for active vibration control, using genetic algorithm, Journal of Sound and Vibration 329 (19) (2010) 1615-1635.

[26] Q. Wang, C. M. Wang, A controllability index for optimal design of piezoelectric actuators in vibration control of beam structures, Journal of Sound and Vibration 242 (3) (2001) 507-518.

[27] K. Hiramoto, H. Doki, G. Obinata, Optimal sensor/actuator placement for active vibration control using explicit solution of algebraic riccati equation, Journal of Sound and Vibration 229 (5) (2000) 1057-1075.

[28] Y. J. Yan, L. H. Yam, Optimal design of number and locations of actuators in active vibration control of a space truss, Smart Material and Structures 11 (2002) 496-503.

[29] T. W. Kim, J. H. Kim, Optimal distribution of an active layer for transient vibration control of a flexible plate, Smart Material and Structures 14 (2005) 904-916.

[30] M. I. Frecker, Recent advances in optimization of smart structures and actuators, Journal of Intelligent Material Systems and Structures, 14 (2003) 207-215.

[31] C. Paulitsch, P. Gardonio, S. J. Elliott, Active vibration control using an inertial actuator with internal damping, The Journal of the Acoustical Society of America 119 (4) (2006) 2131-2140.

[32] L. Benassi, S.J. Elliott, Active vibration isolation using an inertial actuator with local displacement feedback control, Journal of Sound and Vibration 278 (4–5) (2004) 705-724.

[33] S. J. Elliot, M. Serrand, P. Gardonio, Feedback stability limits for active isolation systems with

reactive and inertial actuators, Journal of Vibration and Acoustics, 123 (2) (2001) 250-261.

[34] L. Benassi, S. J. Elliott, P. Gardonio, Active vibration isolation using an inertial actuator with local force feedback control, Journal of Sound and Vibration 276 (2004) 157-179.

[35] I. D. Landau, M. Alma, J. J. Martinez, G. Buche, Adaptive suppression of multiple time-varying unknown vibrations using an inertial actuator, IEEE Transactions on Control Systems Technology, 19 (6) 2011 1327-1338.

[36] Y.P. Xiong, J.T. Xing, W.G. Price, Power Flow Analysis of complex coupled systems by progressive approaches, Journal of Sound and Vibration 239 (2) (2001) 275-295.

[37] C.M. Mak, J.X. Su, A power transmissibility method for assessing the performance of vibration isolation of building services equipment, Applied Acoustics 63 (12) (2002) 1281-1299.

[38] C.M. Mak, J.X. Su, A study of the effect of floor mobility on structure-borne sound power transmission, Building and Environment 38 (3) (2003) 443-455.

[39] F.J. Fahy, P. Gardonio, Sound and structural vibration: radiation, transmission and response, Academic press, London, 2007.

[40] S. F. Ling, Y. Xie, Detecting mechanical impedance of structures using the sensing capability of a piezoceramic inertial actuator, Sensors and Actuators A 93 (2001) 243-249.

[41] G. A. Lesieutre, R. Rusovici, G. H. Koopmann, J. J. Dosch, Modelling and characterization of a piezoceramic inertial actuator, Journal of Sound and Vibration, 261 (2003) 93-107.

[42] S. B. Choi, S. R. Hong, Y. M. Han, Dynamic characteristics of inertial actuator featuring piezoelectric materials: Experimental verification, Journal of Sound and Vibration, 302 (2007) 1048-1056.

[43] Z. Wang, Y. D. Sun, Experimental research on active vibration control of pipe by inertial actuator and adaptive control, in: Proceeding of the 21st International Congress on Sound and Vibration, Beijing, China, 2014.

[44] C.G. Díaz, C. Paulitsch, P. Gardonio, Active damping control unit using a small scale proof mass

electrodynamic actuator, The Journal of the Acoustical Society of America 124 (2) (2008) 886-897.

[45] N. Hirami, Optimal energy absorption as an active noise and vibration control strategy, Journal of Sound and Vibration 200 (3) (1997) 243-259.

[46] O. Bardou, P. Gardonio, S.J. Elliott, R.J. Pinnington, Active power minimization and power absorption in a plate with force and moment excitation, Journal of Sound and Vibration 208 (1) (1997) 111-151.

[47] M. Zilletti, S.J. Elliott, P. Gardonio, Self-tuning control systems of decentralised velocity feedback, Journal of Sound and Vibration 329 (14) (2010) 2738-2750.

[48] M. Zilletti, P. Gardonio, S.J. Elliott, Optimisation of a velocity feedback controller to minimise kinetic energy and maximise power dissipation, Journal of Sound and Vibration 333 (19) (2014) 4405-4414.